Postprint of: Martynow M., Stephan K., Rau S., Guthmuller J., Excited state properties of a series of molecular photocatalysts investigated by time dependent density functional theory, PHYSICAL CHEMISTRY CHEMICAL PHYSICS, Vol. 21, iss. 18 (2019), pp. 9052-9060, DOI: 10.1039/C9CP00335E

Excited state properties of a series of molecular photocatalysts investigated by time dependent density functional theory

Miłosz Martynow[1], Stephan Kupfer[2], Sven Rau[3] and Julien Guthmuller[1]*

[1]*Faculty of Applied Physics and Mathematics, Gdańsk University of Technology, Narutowicza 11/12, 80233 Gdańsk, Poland*

[2]*Institute of Physical Chemistry and Abbe Center of Photonics, Friedrich Schiller University Jena, Helmholtzweg 4, 07743 Jena, Germany*

[3]*Institute of Inorganic Chemistry I, University of Ulm, Albert-Einstein-Allee 11, 89081 Ulm, Germany*

Abstract

Time dependent density functional theory calculations are applied on a series of molecular photocatalysts of the type $[(tbbpy)_2M1(tpphz)M2X_2]^{2+}$ (M1=Ru, Os ; M2=Pd, Pt ; X=Cl, I) in order to provide information concerning the photochemistry occurring upon excitation of the compounds in the visible region. To this aim, the energies, oscillator strengths and orbital characters of the singlet and triplet excited states are investigated. The structural modifications of the complexes have a strong impact on the excited states properties. In particular, it is found that the main differences concern the energies of the charge-separated and metal-centered states. The analysis of these differences provides general trends for the efficiency of population transfers between the states, particularly regarding the charge separation and electron recombination processes.

1. Introduction

The development of devices and materials for the conversion of solar energy into energy-rich chemicals (*i.e.* solar fuel) is a highly active field of research in chemistry and physics. In particular, extensive efforts are conducted to develop photocatalytic systems for the splitting of water into molecular hydrogen and oxygen. In this context, several hydrogen-evolving molecular photocatalysts were reported in the last decades[1,2,3,4,5,6,7,8,9]. These systems typically consist of a photosensitizer, a bridging ligand (BL) and a catalytic center, where the molecular hydrogen is formed. The design and improvement of these so-called three-component systems requires a precise understanding of the interplay between the light absorption, the electron transfer processes and the catalytic turnover. To this aim, theoretical methods provide a means to investigate the molecular properties governing the photochemistry of these compounds (see *e.g.*[10,11,12]).

This work focuses on the excited state properties of a series of molecular photocatalysts $[(tbbpy)_2M1(tpphz)M2X_2]^{2+}$ (tbbpy=4,4'-di-*tert*-butyl-2,2'-bipyridine, tpphz=tetrapyrido[3,2-a:2',3'-c:3'''-h:2''',3'''-j]phenazine) (Figure 1), which will be denoted as **M1M2X$_2$**, as well as of their precursors $[(tbbpy)_2M1(tpphz)]^{2+}$, denoted **M1**. These systems were introduced by the group of Sven Rau[1,7,8,13] and have been the subject of several experimental and computational studies[14,15,16,17,18,19] to understand their photophysical properties and photocatalytic activity. In particular, the resonance Raman spectrum, the triplet excited states properties and the electron transfer processes were investigated theoretically[16,18,11] for **RuPdCl$_2$**, whereas only the absorption spectra were calculated[7,8,17] for **RuPtCl$_2$** and **RuPtI$_2$**. To realize light-driven hydrogen production, the catalytic center ($M2X_2$) must undergo double reduction. For this class of molecular photocatalysts, the commonly accepted mechanism for the first photo-induced electron transfer from the photosensitizer toward the catalytic center involves the following steps: (i) photoexcitation in the first absorption band leads to the population of metal-to-ligand charge-transfer (MLCT) states localized on the tpphz and bpy ligands, (ii) ultrafast intersystem crossing (ISC) and excited state relaxation processes leading to the population of triplet MLCT state(s) localized on the tpphz

bridging ligand, and (iii) electron transfer to the catalytic center leading to the reduction of M2 and thus, to the formation of a charge-separated (CS) species. Information concerning step (i) can be obtained from the singlet excited states properties, whereas the steps (ii) and (iii) are determined by the triplet excited states. In particular, step (ii) depends on the triplet states initially populated through ISC from the singlet states, and step (iii) involves population transfers between different triplet states. Therefore, the goals of this study are (i) to identify the energetic positions and electronic characters of the excited states involved in the photochemistry, (ii) to investigate the correlation between the introduced structural modifications of the photocatalysts and the excited states properties, and (iii) to establish preliminary trends concerning the efficiency of population transfers between the states, particularly regarding the charge separation and electron recombination processes.

The paper is organized as follows: section 2 presents the quantum chemistry methods. Section 3.1 reports the absorption spectra and singlet excited states properties. Section 3.2 describes and discussed the emission wavelengths and triplet excited states properties. Finally, Section 4 provides a conclusion.

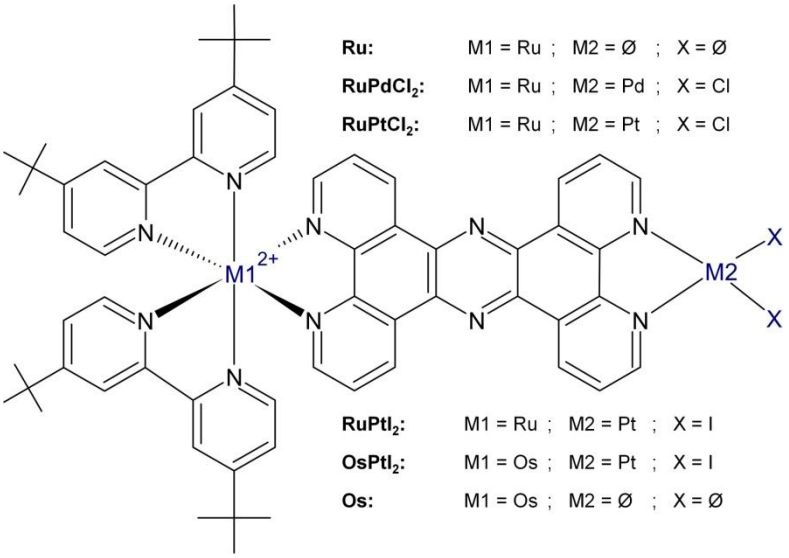

Figure 1. Structure and employed nomenclature of the investigated systems.

2. Computational methods

All quantum chemical calculations were performed with the Gaussian 09 program[20], which provided the structural and electronic properties of the different complexes. To reduce the computational cost of the calculations without affecting the properties, the structures of the complexes were simplified by replacing the *tert*-butyl groups by methyl groups (Figure 1). The equilibrium geometries of the singlet ground state (S_0) and of the MLCT triplet state T_{BL1_YZ} were obtained by means of density functional theory (DFT) using the B3LYP exchange-correlation (XC) functional[21,22]. Harmonic vibrational frequencies were computed to confirm that the optimized structures correspond to minima on the potential energy surface. The relativistic effective core potentials MWB[23] were used with their basis sets for the ruthenium, palladium, iodine, osmium and platinum atoms. These effective core potentials describe the 28, 28, 46, 60 and 60 core electrons of Ru, Pd, I, Os and Pt, respectively. The 6-31G(d) basis set[24] was employed for the main group elements. The vertical excitation energies, oscillator strengths and electronic characters of the 200 lowest singlet and 200 lowest triplet excited states were calculated with time dependent DFT (TDDFT). These calculations were performed at the S_0 and T_{BL1_YZ} geometries using the same XC functional, basis sets and core potentials. This computational protocol was already successfully applied to simulate the UV-vis absorption and resonance Raman spectra, the spectro-electrochemistry properties and the electron transfer dynamics in structurally related transition metal complexes[16,17,18,10,11]. In particular, it has shown to provide a balanced description of the ground and excited states properties for electronic states of different nature, *i.e.*, MLCT, intra-ligand charge transfer, intra-ligand, ligand-to-ligand charge transfer, ligand-to-metal charge transfer and metal-centered states. The effects of the interaction with a solvent (acetonitrile, ε = 35.688, n = 1.344) were taken into account for the ground state and the excited states properties by the integral equation formalism of the polarizable continuum model[25] (IEFPCM). The nonequilibrium procedure of solvation was used for the calculation of the vertical singlet-singlet and singlet-triplet

excitation energies at the S_0 and T_{BL1_YZ} geometries, which is well-adapted for processes where only the fast reorganization of the electronic distribution of the solvent is important.

3. Results

3.1. Absorption spectra and singlet excited states

The simulated absorption spectra of the six investigated systems, including the transitions to the 200 lowest singlet excited states, are reported on Figure 2. The absorption spectrum of each compound presents a similar shape and is composed of a MLCT band covering the visible region (*i.e.* from 600 to 400 nm) and involving excitations from the ruthenium or osmium centers. Additionally, intense bands are obtained in the UV domain and are associated with excited states of different characters, *i.e.* intra-ligand (IL) states, ligand-to-ligand charge transfer states and MLCT states involving the catalytic centers, namely Pd or Pt. In the photocatalytic process[1,7,8], the initial photoexcitation occurs in the visible range, which leads to the population of MLCT states. The calculations show that the MLCT band consists mainly of a superposition of six to eight MLCT states having non-negligible oscillator strengths (see Figure 2 and the Tables S1-S6). In the longer wavelength range, each system displays a low-lying MLCT state toward the bridging ligand (S_{tpphz}) that involves a transition from the d_{XZ}(M1) orbital to the π^*_{BL1} orbital (Figure 3). This state features an oscillator strength of about 0.12 in **Ru** and **Os**, whereas its intensity is decreased by a factor of two (f of about 0.06) in the other systems (Table 1). Additionally, the excitation energy of S_{tpphz} is shifted to lower energies (by about 0.2 eV) going from the precursors **Ru** and **Os** to the molecular photocatalysts **RuM2X$_2$** and **OsPtI$_2$**, respectively. Therefore, the observed decrease of the oscillator strength from the precursors to the photocatalysts can be partially attributed to the energetic stabilization of the low-lying MLCT state, S_{tpphz}. This shows that coordination of the catalytic center ($M2X_2$) influences the tpphz MLCT states properties. The shorter wavelength range of the MLCT band is dominated by transitions to the bpy ligands. In particular, each system presents an intense bpy MLCT state (S_{bpy}) having an oscillator strength comprised between 0.14 and 0.16

(Table 1). The S_{bpy} state involves transitions from the orbitals d_{XZ}(M1) and d_{XY}(M1) to the orbitals π^*_{bpy2} and π^*_{bpy1}, respectively (Figures 2-3 and Table 1). Its transition wavelength is located close to 420 nm is all Ru-based systems, whereas it is red-shifted to about 445 nm in the two Os-based compounds. Hence, the coordination of the catalytic center has a negligible effect on the bpy MLCT excitation energies, whereas the replacement of ruthenium by osmium leads to a decrease of about 0.2 eV of the excitation energies for both S_{tpphz} and S_{bpy} states (Table 1). The other excited states (see Tables S1-S6) contributing to the MLCT band involve transitions to the π^*_{BL2} and π^*_{BL4} orbitals as well as to the bpy ligands (*i.e.* π^*_{bpy1} and π^*_{bpy2} orbitals). These states are mainly located in-between the S_{tpphz} and S_{bpy} states and often present a strong mixing of transitions toward the tpphz and bpy ligands.

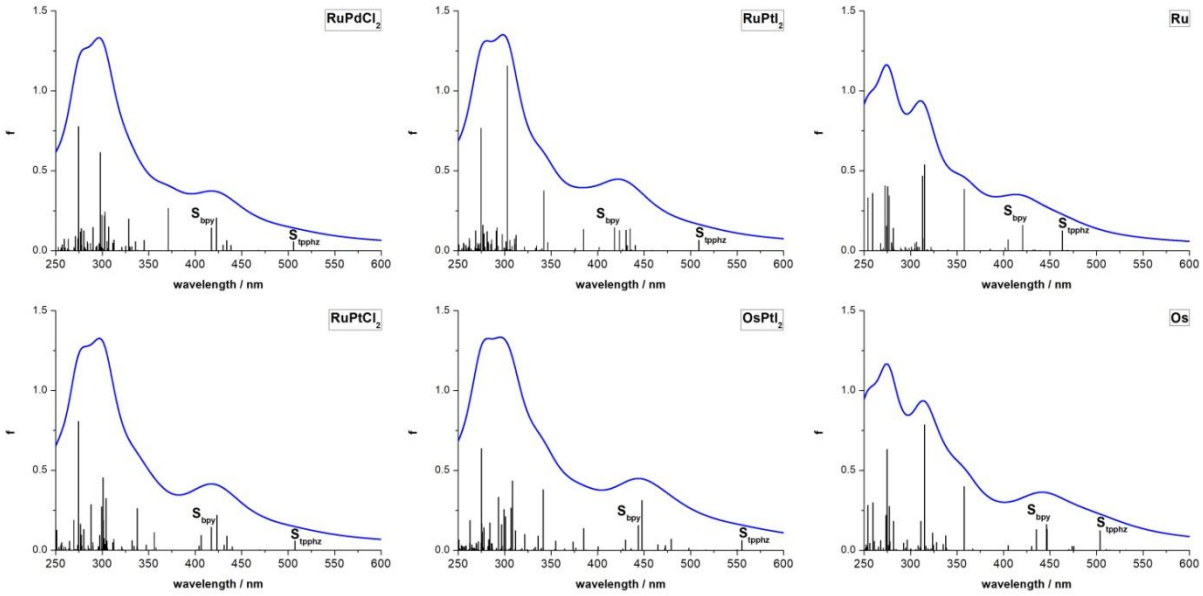

Figure 2. Simulated absorption spectra and oscillator strengths (f). A Lorentzian function with a full width at half maximum (FWHM) of 4000 cm^{-1} is employed to broaden the transitions.

Table 1. Vertical excitation energies (VEE), wavelengths (λ), oscillator strengths (f) and singly-excited configurations of the S_{tpphz} and S_{bpy} singlet excited states calculated at the S_0 geometry.

State	Transition	Weight (%)[a]	VEE (eV)	λ (nm)	f
Ru					
S_{tpphz}	$d_{XZ}(Ru) \rightarrow \pi^*_{BL1}$ $d_{XZ}(Ru) \rightarrow \pi^*_{BL4}$	82 11	2.68	463	0.126
S_{bpy}	$d_{XY}(Ru) \rightarrow \pi^*_{bpy1}$ $d_{XZ}(Ru) \rightarrow \pi^*_{bpy2}$	47 40	2.95	421	0.158
$RuPdCl_2$					
S_{tpphz}	$d_{XZ}(Ru) \rightarrow \pi^*_{BL1}$	96	2.45	506	0.058
S_{bpy}	$d_{XZ}(Ru) \rightarrow \pi^*_{bpy2}$ $d_{XY}(Ru) \rightarrow \pi^*_{bpy1}$	52 44	2.97	418	0.142
$RuPtCl_2$					
S_{tpphz}	$d_{XZ}(Ru) \rightarrow \pi^*_{BL1}$	95	2.44	507	0.058
S_{bpy}	$d_{XZ}(Ru) \rightarrow \pi^*_{bpy2}$ $d_{XY}(Ru) \rightarrow \pi^*_{bpy1}$	51 44	2.97	417	0.144
$RuPtI_2$					
S_{tpphz}	$d_{XZ}(Ru) \rightarrow \pi^*_{BL1}$	95	2.44	508	0.065
S_{bpy}	$d_{XZ}(Ru) \rightarrow \pi^*_{bpy2}$ $d_{XY}(Ru) \rightarrow \pi^*_{bpy1}$	53 42	2.97	418	0.144
$OsPtI_2$					
S_{tpphz}	$d_{XZ}(Os) \rightarrow \pi^*_{BL1}$	93	2.23	555	0.061
S_{bpy}	$d_{XZ}(Os) \rightarrow \pi^*_{bpy2}$ $d_{XY}(Os) \rightarrow \pi^*_{bpy1}$	60 34	2.79	443	0.157
Os					
S_{tpphz}	$d_{XZ}(Os) \rightarrow \pi^*_{BL1}$ $d_{XZ}(Os) \rightarrow \pi^*_{BL4}$	80 14	2.46	503	0.124
S_{bpy}	$d_{XZ}(Os) \rightarrow \pi^*_{bpy2}$ $d_{XY}(Os) \rightarrow \pi^*_{bpy1}$	49 41	2.78	446	0.163

[a] Weights larger than 10%.

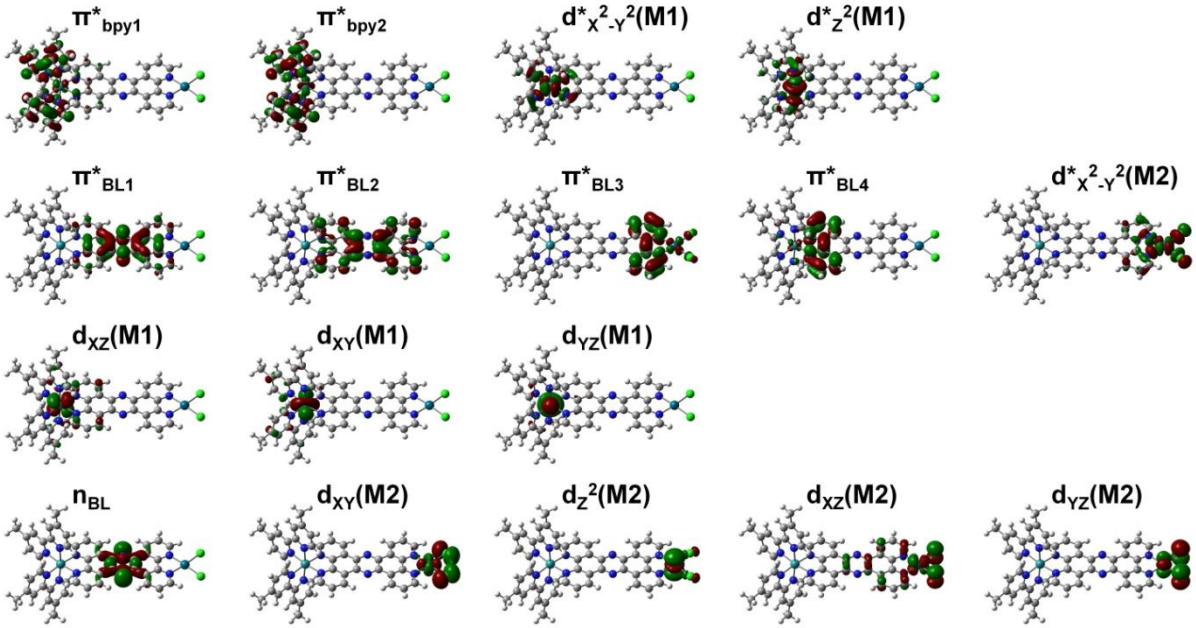

Figure 3. Frontier orbitals (**$RuPdCl_2$** at the S_0 geometry) and employed nomenclature.

The comparison between the theoretical and experimental absorption maxima of the MLCT band is reported in Table 2. Overall, the calculations overestimate the MLCT excitation energies of the Ru-based complexes by about 0.2 eV, which is a typical accuracy for TDDFT computations of MLCT singlet excited states[26,27,28,29]. The calculated absorption maxima of the Ru-based compounds have comparable values, which are comprised between 413 and 422 nm. This result is in agreement with the experimental data, which shows nearby values comprised between 445 and 448 nm. The similarity of the λ_{Abs} values for the different Ru-based complexes can be explained by the fact that the MLCT band maxima are mainly determined by the positions of the bpy MLCT states, which remain unaltered by the attachment or replacement of the catalytic center (Table 1). The calculated absorption maxima of the Os-based compounds are red-shifted by about 0.2 eV with respect to the Ru-based compounds. The experimental MLCT absorption band[13] of the Os complexes is broader than for the Ru complexes. In particular, it displays two maxima at 430 and 485 nm for **$OsPtI_2$** and at 435 and 497 nm for **Os**. Thus, the calculated values of 444 and 441 nm for **$OsPtI_2$** and **Os**, respectively, are in-between the experimental maxima. It should be mentioned that the origin of the broader structure for the MLCT absorption band of the Os-based compounds is likely to involve spin-orbit coupling effects, in particular, in the longer wavelength region[13]. These effects are not taken into account in the present calculations.

Table 2. Absorption maxima (λ_{Abs}, E_{Abs}) and vertical emission wavelengths (λ_{Em}) of the different systems.

System	λ_{Abs} (nm) [E_{Abs} (eV)]		λ_{Em} (nm)	
	Cal.	Exp.[a]	Cal.	Exp.[a]
Ru	413 [3.00]	445[b] [2.79]	646	638[b]
$RuPdCl_2$	417 [2.97]	445[b] [2.79]	637	650[b] (very weak)
$RuPtCl_2$	417 [2.97]	448[c] [2.77]	638	-
$RuPtI_2$	422 [2.94]	445[d,e] [2.79]	640	-
$OsPtI_2$	444 [2.79]	430[e] [2.88]	741	-
Os	441 [2.81]	485[e] [2.56] 435[f] [2.85] 497[f] [2.49]	739	740[f]

[a] Measured in acetonitrile. [b] From reference[1]. [c] From reference[7]. [d] From reference[8]. [e] From reference[30]. [f] From reference[13].

3.2. Description of the triplet excited states

The geometry of the lowest triplet state of the precursors (**Ru** and **Os**) was optimized with DFT. This state corresponds to a MLCT excitation toward the bridging ligand and mainly involves a transition between the HOMO orbital d_{YZ}(M1) and the LUMO orbital π^*_{BL1} (Figure 3). In the following this state is called T_{BL1_YZ}. Then, the vertical emission wavelengths were calculated with TDDFT assuming that the emission occurs from the T_{BL1_YZ} state. The obtained values of 646 and 739 nm are in excellent agreement with the experimental values of 638 and 740 nm for **Ru** and **Os**, respectively (Table 2). These results show that replacing the Ru atom by an Os atom stabilizes the MLCT triplet state T_{BL1_YZ} by about 0.25 eV. Additionally, the geometry of the T_{BL1_YZ} state and its associated emission wavelength were also calculated for the molecular photocatalysts (Table 2). However, the emission of these systems is quenched in experiment, only a very weak emission at 650 nm was reported[1] for **$RuPdCl_2$**. This latter value is in agreement with the calculated result at 637 nm (*i.e.* deviation of 0.04 eV). The absence or decrease of emission in the molecular photocatalysts is likely ascribed to the competition between radiative and non-radiative excited state relaxation channels, which become accessible upon introduction of the catalytic center. In particular, for **$RuPdCl_2$** and structurally related systems[11,31], hole transfer processes, *i.e.* population transfers from T_{BL1_YZ} to low-lying M2-centered states, were found to be prominent relaxation channels.

In the next step the singlet-triplet transitions were calculated with TDDFT both at the S_0 and T_{BL1_YZ} geometries (see Figures 4-5 and Tables S7-S12). The lowest triplet states expected to play a role in the photochemistry were labeled following their singly-excited orbital configurations. The employed nomenclature includes: (i) twelve MLCT states involving transitions from the orbitals d_{XZ}(M1), d_{XY}(M1) and d_{YZ}(M1) to the bridging ligand orbitals π^*_{BL1}, π^*_{BL2}, π^*_{BL3} and π^*_{BL4} (*i.e.* T_{BL1_XZ}, T_{BL1_XY}, T_{BL1_YZ}, T_{BL2_XZ}, T_{BL2_XY}, T_{BL2_YZ}, T_{BL3_XZ}, T_{BL3_XY}, T_{BL3_YZ}, T_{BL4_XZ}, T_{BL4_XY} and T_{BL4_YZ}), (ii) six MLCT states involving transitions from the orbitals d_{XZ}(M1), d_{XY}(M1) and d_{YZ}(M1) to the bpy ligands orbitals π^*_{bpy1} and π^*_{bpy2} (*i.e.* T_{bpy1_XZ}, T_{bpy1_XY}, T_{bpy1_YZ}, T_{bpy2_XZ},

T_{bpy2_XY} and T_{bpy2_YZ}), (iii) four M2-centered states involving transitions from the orbitals d_{XY}(M2), $d_Z{}^2$(M2), d_{XZ}(M2) and d_{YZ}(M2) to the orbital $d^*_{X^2-Y^2}$(M2) (*i.e.* T_{M2_XY}, $T_{M2\_Z^2}$, T_{M2_XZ} and T_{M2_YZ}), (iv) three charge-separated states involving transitions from the orbitals d_{XZ}(M1), d_{XY}(M1) and d_{YZ}(M1) to the orbital $d^*_{X^2-Y^2}$(M2) (*i.e.* T_{CS_XZ}, T_{CS_XY} and T_{CS_YZ}), and (v) six M1-centered states involving transitions from the orbitals d_{XZ}(M1), d_{XY}(M1) and d_{YZ}(M1) to the orbitals $d^*_{X^2-Y^2}$(M1) and $d^*_{Z^2}$(M1) (*i.e.* $T_{M1\_XZ\_X^2Y^2}$, $T_{M1\_XZ\_Z^2}$, $T_{M1\_XY\_X^2Y^2}$, $T_{M1\_XY\_Z^2}$, $T_{M1\_YZ\_X^2Y^2}$ and $T_{M1\_YZ\_Z^2}$). Additionally, IL states localized on the bridging ligand and MLCT states involving the M2 atom are present among the previously considered triplet excited states (see Tables S7-S12). In order to describe their general behavior, two such states were included in the analysis, namely, (i) an IL state involving a transition from the symmetric lone pair of the phenazine nitrogen atoms (n_{BL}) to the orbital π^*_{BL1} (*i.e.* T_{IL}) and (ii) a MLCT state involving mainly a transition from the orbital d_{XZ}(M2) to the orbital π^*_{BL1} (*i.e.* T_{MLCT}).

Figure 4 displays the excited state energies of the six complexes calculated at the ground state geometry (S_0). The positions of the S_{tpphz} and S_{bpy} states indicate the energy range of the initial photoabsorption. The evolution of these states between the compounds was already described in section 3.1.. For clarity only the energies of the MLCT (T_{BL1}, T_{BL2}, T_{BL3}, T_{BL4} and T_{bpy1}) and charge-separated (T_{CS}) states originating from the d_{YZ}(M1) orbital are reported. Additionally, only the energies of the two metal-centered states T_{M2_YZ} and $T_{M1\_YZ\_X^2Y^2}$ are given on Figure 4. This choice is justified by the fact that the other MLCT, CS and metal-centered states display a very similar energetic behavior (see Figures S1-S2 and Tables S7-S12).

For these systems, it is well-established[14,15,7,8,11] that after photoexcitation to the singlet excited states, an ultrafast population transfer to the triplet manifold occurs by ISC. This transfer most likely populates the different T_{BL} and T_{bpy} states, because these states have similar energies and orbital characters as the populated singlet states. In particular, an excitation in S_{tpphz} is expected to populate predominantly the T_{BL1} states[11,18], whereas excitation in S_{bpy} could in principle lead to the population of the T_{bpy} states and in a further step to the population of all the T_{BL} states (with the

exception of T_{BL3} states in **Ru** and **Os**, which are much higher in energy). In this way, the T_{bpy} states lying in-between the T_{BL} states might play the role of electron reservoirs as was recently shown in the photochemistry of related compounds[9,32,33]. In addition to the S_0 geometry, the triplet excited state energies were also calculated at the T_{BL1_YZ} geometry (Figure 5). The T_{BL1_YZ} state provides the geometry of a typical T_{BL} state that is likely populated through ISC from the singlet states. It is directly seen by comparison of the Figures 4 and 5 that the relative energy evolution of the triplet states is very similar at the S_0 and T_{BL1_YZ} geometries (see also Figures S1-S3 for the other states). At the S_0 geometry, the lowest triplet state of **Ru** and **Os** is dominated by a transition to the orbital π^*_{BL4}, whereas the lowest MLCT state is T_{BL1_YZ} for the other geometry and systems. Moreover, the T_{BL} states are mainly stabilized when going from the precursors to the molecular photocatalysts. In particular, the T_{BL3} state, which is localized close to the catalytic center, presents the largest stabilization. These observations show that the catalytic center influences significantly the bridging ligand MLCT triplet states. These changes are expected to facilitate the electron transfer steps toward the catalytic center. Nevertheless, the results for the Ru-based compounds show that changing the type of catalytic centers does not impact the T_{BL} states energies. As could be anticipated, the energies of the T_{bpy} states remain nearly unaffected by the catalytic center. However, similarly to the singlet states (section 3.1) all the triplet MLCT states are stabilized going from the Ru-based compounds to the Os-based compounds.

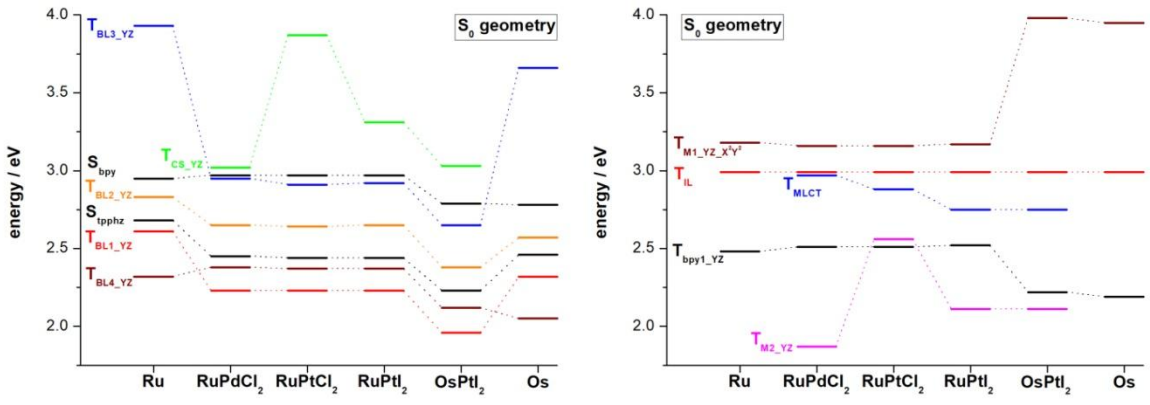

Figure 4. Excited states energy diagram calculated at the S_0 geometry.

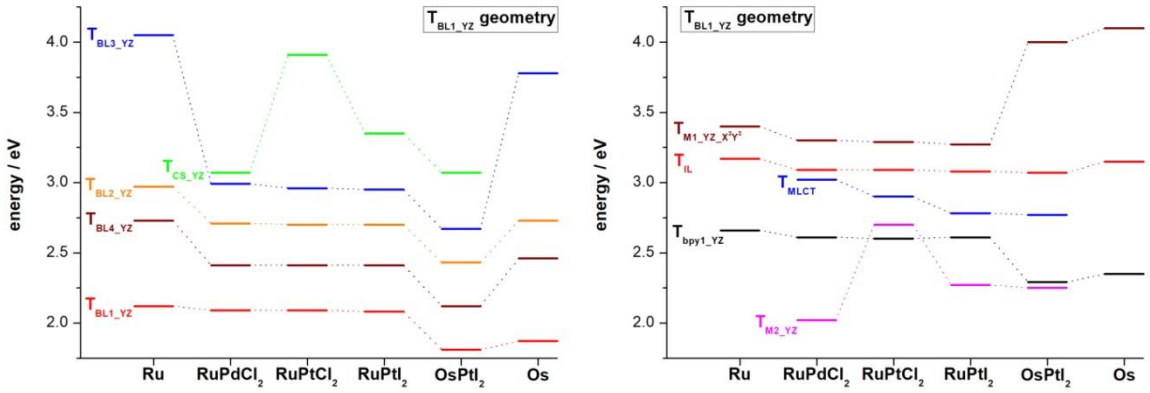

Figure 5. Excited states energy diagram calculated at the T_{BL1_YZ} geometry. The energies are given with respect to the energy of the S_0 state at the S_0 geometry.

Assuming that a T_{BL} state is populated, which describes a hole at M1 and a reduced tpphz ligand, the accessibility of different pathways is discussed based on the relative energies of the states. The completion of a first electron transfer to the catalytic center requires the population of the T_{CS} states. As can be seen from the Figures 4 and 5, the energies of such state strongly depend on the catalytic center. The most stable T_{CS} states are obtained for **$RuPdCl_2$**, whereas the replacement of the palladium by platinum (**$RuPtCl_2$**) produces the T_{CS} states with the highest energy. Then, the exchange of the chlorides by iodides (**$RuPtI_2$**) generates T_{CS} states with energies in-between those of **$RuPdCl_2$** and **$RuPtCl_2$**. The relative energies of the T_{BL} and T_{CS} states in **$OsPtI_2$** is very similar to **$RuPtI_2$**, the main difference corresponds to a global stabilization of all the states in **$OsPtI_2$** with respect to **$RuPtI_2$**. These differences are consequently expected to affect the accessibility of the T_{CS} states from the T_{BL} states. According to the calculated relative energies the electron transfer efficiency of the $T_{BL} \rightarrow T_{CS}$ process should decrease in the order **$RuPdCl_2$** > **$RuPtI_2$**, **$OsPtI_2$** > **$RuPtCl_2$** and is most likely to occur from the T_{BL3} states. It can be mentioned that these results correlate qualitatively with the measured catalytic turnover numbers (TONs) for hydrogen generation. Indeed, maximum TON values of 238, of 276 and of less than 10 were reported[34,7,8] for the Ru-based photocatalysts **$RuPdCl_2$**, **$RuPtI_2$** and **$RuPtCl_2$**, respectively. This

indicates that the low TON of **$RuPtCl_2$** might be due to its high-energy T_{CS} states, whereas the stabilization of the T_{CS} states in **$RuPdCl_2$** and **$RuPtI_2$** is associated with larger TONs.

The possibility of a charge recombination from a T_{BL} state is now discussed. From an energetic point of view the most likely recombination processes correspond to $T_{BL}\rightarrow T_{M2}$ transfers. Such a population transfer describes an electron recombination from the tpphz ligand toward M1 in conjunction with an energy transfer toward M2. In the case of **$RuPdCl_2$**, the $T_{BL1}\rightarrow T_{Pd}$ processes were recently investigated using the Marcus theory[11]. It was found that the T_{Pd} states are very efficiently populated with estimated time constants below 1 ps. It was also speculated that these states might be responsible for a non-radiative relaxation channel to the S_0 ground state, which could provide an explanation for the quenching of emission in the molecular photocatalysts. Such quenching can be further rationalized by means of the population of CS states (T_{CS}), which are localized below the T_{BL} states upon equilibration (*i.e.* at the T_{CS} geometry) in **$RuPdCl_2$** and in a structurally related ruthenium-cobalt photocatalyst[11,10]. Additionally, it was proposed that the population of T_{Pd} states can lead to the alteration of the catalytic center by inducing Cl^- dissociation. The relative stability of the T_{M2} states with respect to the T_{BL} states in the different systems (Figures 4 and 5) suggests that the efficiency of the $T_{BL}\rightarrow T_{M2}$ transfers should decrease in the order **$RuPdCl_2$** > **$RuPtI_2$** > **$OsPtI_2$** > **$RuPtCl_2$**. If the T_{M2} states are assumed to play a role in the degradation of the catalytic center, this results is in agreement with the experimental observations that the **$RuPdCl_2$** system undergoes an alteration of the catalytic center[7], which results in the formation of metal colloids, whereas the other compounds based on a platinum catalytic center are stable during the catalysis[8]. The stability of the Pt-based catalytic centers could also originate from larger Pt-Cl and Pt-I bond strengths in comparison to the Pd-Cl bond.

Another possible recombination mechanism corresponds to $T_{BL}\rightarrow T_{M1}$ transfers, which describe an electron recombination from the tpphz ligand toward M1. However, the T_{M1} states are higher in energy than the T_{BL} states in all the molecular photocatalysts, which implies that such recombination processes should be less likely to occur than the $T_{BL}\rightarrow T_{M2}$ transfers. It is also found

that the T_{M1} states are much higher in **$OsPtI_2$** (more than 1 eV above the T_{BL3} states) in comparison to the Ru-based compounds. This difference should lead to lower recombination via T_{Os} states in **$OsPtI_2$**.

Other triplet excited states are present in the vicinity of the T_{BL} states. Figures 4 and 5 report the energies of an intra-ligand state T_{IL}, which involves a transition from the orbital n_{BL} to the orbital π^*_{BL1} (Figure 3). The $T_{BL} \rightarrow T_{IL}$ transfers describe an electron recombination from tpphz toward M1, while the tpphz bridging ligand remains in an excited state. Due to the nearly identical energy of T_{IL} in the different molecular photocatalysts and of its position located just above the T_{BL3} states, a recombination via this state appears more likely in Ru-based compounds than in **$OsPtI_2$**. Finally, the evolution of the MLCT state T_{MLCT} is considered, which involves mainly a transition from the orbital d_{XZ}(M2) to the orbital π^*_{BL1} (see Tables S7-S12). The energy of the state is stabilized in the order **$RuPdCl_2$** > **$RuPtCl_2$** > **$RuPtI_2$** and **$OsPtI_2$** due to the replacement of the catalytic center. The $T_{BL} \rightarrow T_{MLCT}$ transfers can be described as the transfer of a hole from M1 toward M2 and therefore involves an electron recombination on the M1 center. This state is in energetic proximity to the T_{BL} states, indicating that it might lead to recombination processes, which should be more likely to occur in **$RuPtI_2$** and **$OsPtI_2$** due to the lower energy of T_{MLCT} in these systems.

4. Conclusion

The properties of the singlet and triplet excited states of a series of precursors and molecular photocatalysts were investigated by DFT and TDDFT calculations. The theoretical results show that the first absorption bands of the different systems consist mainly of a superposition of six to eight MLCT states with non-negligible oscillator strengths. The longer wavelength range of the absorption spectrum displays mostly MLCT transitions toward the tpphz bridging ligand, whereas the shorter wavelength range of the MLCT band is dominated by transitions toward the bpy ligands. The comparison with experimental data shows that the calculations reproduce the main features of

the absorption spectra and that the obtained emission wavelengths are in excellent agreement with the experimental values. This observation together with previous studies[10,11,18,35,36,37] confirms the adequacy of the computational methods to investigate the excited states properties.

A comparison of the triplet excited states energies was performed in order to identify prominent relaxation channels accessible upon photoexcitation and to investigate their dependency with respect to the substitution pattern. In particular, it was found that the attachment of the catalytic centers, namely $PdCl_2$, $PtCl_2$ and PtI_2 has a negligible effect on the MLCT excitations toward the bpy ligands, whereas it leads to the stabilization of the MLCT excitations toward the tpphz ligand. Additionally, the replacement of the Ru atom by an Os atom stabilizes all singlet and triplet MLCT states by about 0.2-0.3 eV. However, the principal differences between the molecular photocatalysts concern the changes in energies for the T_{CS}, T_{M2} and T_{M1} states. Thus, assuming that a T_{BL} state is populated, the following conclusions can be drawn regarding the electron transfer efficiencies, (i) the efficiency of the $T_{BL} \rightarrow T_{CS}$ process should decrease in the order **$RuPdCl_2$** > **$RuPtI_2$**, **$OsPtI_2$** > **$RuPtCl_2$** and is most likely to occur from the T_{BL3} states, (ii) the most prominent recombination processes correspond to $T_{BL} \rightarrow T_{M2}$ transfers and their efficiency is expected to decrease in the order **$RuPdCl_2$** > **$RuPtI_2$** > **$OsPtI_2$** > **$RuPtCl_2$**, and (iii) the $T_{BL} \rightarrow T_{M1}$ recombination processes are less likely to occur than the $T_{BL} \rightarrow T_{M2}$ transfers, and their efficiency should be strongly decreased in **$OsPtI_2$** in comparison to the Ru-based molecular photocatalysts. To confirm the obtained trends, further studies should focus on the optimization of the excited states geometries and in the simulation of rate constants for the competitive photo-induced electron transfer processes using for example the semi-classical Marcus theory[10,11]. Such investigations will provide valuable information to elucidate the mechanism associated to the catalytic activity and finally to the formation of molecular hydrogen.

Acknowledgments

This work is supported by the Narodowe Centrum Nauki (NCN) (project No. 2014/14/M/ST4/00083). The calculations were performed at the Wrocław Centre for Networking and Supercomputing (grant No. 384) and at the Academic Computer Centre TASK in Gdańsk. Furthermore, we are grateful for the support of the COST Action CM1202 Perspect-H2O.

References

1 S. Rau, B. Schäfer, D. Gleich, E. Anders, M. Rudolph, M. Friedrich, H. Görls, W. Henry and J. G. Vos, A Supramolecular Photocatalyst for the Production of Hydrogen and the Selective Hydrogenation of Tolane, *Angew. Chem. Int. Ed.*, 2006, **45**, 6215–6218.

2 H. Ozawa, M. A. Haga and K. Sakai, A photo-hydrogen-evolving molecular device driving visible-light-induced EDTA-reduction of water into molecular hydrogen, *J. Am. Chem. Soc.*, 2006, **128**, 4926–4927.

3 E. S. Andreiadis, M. Chavarot-Kerlidou, M. Fontecave and V. Artero, Artificial photosynthesis: From molecular catalysts for light-driven water splitting to photoelectrochemical cells, *Photochem. Photobiol.*, 2011, **87**, 946–964.

4 V. Artero, M. Chavarot-Kerlidou and M. Fontecave, Splitting water with cobalt, *Angew. Chemie - Int. Ed.*, 2011, **50**, 7238–7266.

5 Y. Halpin, M. T. Pryce, S. Rau, D. Dini and J. G. Vos, Recent progress in the development of bimetallic photocatalysts for hydrogen generation, *Dalt. Trans.*, 2013, **42**, 16243–16254.

6 L. Hammarström, Accumulative Charge Separation for Solar Fuels Production: Coupling Light-Induced Single Electron Transfer to Multielectron Catalysis, *Acc. Chem. Res.*, 2015, **48**, 840–850.

7 M. G. Pfeffer, B. Schäfer, G. Smolentsev, J. Uhlig, E. Nazarenko, J. Guthmuller, C. Kuhnt, M. Wächtler, B. Dietzek, V. Sundström and S. Rau, Palladium versus Platinum: The Metal in the Catalytic Center of a Molecular Photocatalyst Determines the Mechanism of the Hydrogen Production with Visible Light, *Angew. Chem. Int. Ed.*, 2015, **54**, 5044–5048.

8 M. G. Pfeffer, T. Kowacs, M. Wächtler, J. Guthmuller, B. Dietzek, J. G. Vos and S. Rau, Optimization of hydrogen-evolving photochemical molecular devices, *Angew. Chem. Int. Ed.*, 2015, **54**, 6627–6631.

9 Q. Pan, L. Freitag, T. Kowacs, J. C. Falgenhauer, J. P. Korterik, D. Schlettwein, W. R. Browne, M. T. Pryce, S. Rau, L. González, J. G. Vos and A. Huijser, Peripheral ligands as electron storage reservoirs and their role in enhancement of photocatalytic hydrogen generation, *Chem. Commun.*, 2016, **52**, 9371–9374.

10 A. Koch, D. Kinzel, F. Dröge, S. Gräfe and S. Kupfer, Photochemistry and Electron Transfer Kinetics in a Photocatalyst Model Assessed by Marcus Theory and Quantum Dynamics, *J. Phys. Chem. C*, 2017, **121**, 16066–16078.

11 M. Staniszewska, S. Kupfer and J. Guthmuller, Theoretical Investigation of the Electron-Transfer Dynamics and Photodegradation Pathways in a Hydrogen-Evolving Ruthenium-Palladium Photocatalyst, *Chem. Eur. J.*, 2018, **24**, 11166–11176.

12 J. Cao and Y. Zhou, Excited state relaxation processes of H2-evolving Ru–Pd supramolecular photocatalysts containing a linear or non-linear bridge: a DFT and TDDFT study, *Phys. Chem. Chem. Phys.*, 2017, **19**, 11529–11539.

13 J. Habermehl, D. Sorsche, P. Murszat and S. Rau, Making Use of Obstacles: Alternative Synthetic Approaches towards Osmium(II)-Based Photochemical Molecular Devices, *Eur. J. Inorg. Chem.*, 2016, 3423–3428.

14 S. Tschierlei, M. Presselt, C. Kuhnt, A. Yartsev, T. Pascher, V. Sundström, M. Karnahl, M. Schwalbe, B. Schäfer, S. Rau, M. Schmitt, B. Dietzek and J. Popp, Photophysics of an Intramolecular Hydrogen-Evolving Ru–Pd Photocatalyst, *Chem. Eur. J.*, 2009, **15**, 7678–

7688.

15 S. Tschierlei, M. Karnahl, M. Presselt, B. Dietzek, J. Guthmuller, L. González, M. Schmitt, S. Rau and J. Popp, Photochemical Fate: The First Step Determines Efficiency of H2 Formation with a Supramolecular Photocatalyst, *Angew. Chem. Int. Ed.*, 2010, **49**, 3981–3984.

16 J. Guthmuller and L. González, Simulation of the resonance Raman intensities of a ruthenium-palladium photocatalyst by time dependent density functional theory., *Phys. Chem. Chem. Phys.*, 2010, **12**, 14812–14821.

17 L. Zedler, J. Guthmuller, I. Rabelo de Moraes, S. Kupfer, S. Krieck, M. Schmitt, J. Popp, S. Rau and B. Dietzek, Resonance-Raman spectro-electrochemistry of intermediates in molecular artificial photosynthesis of bimetallic complexes, *Chem. Commun.*, 2014, **50**, 5227–5229.

18 M. Wächtler, J. Guthmuller, S. Kupfer, M. Maiuri, D. Brida, J. Popp, S. Rau, G. Cerullo and B. Dietzek, Ultrafast intramolecular relaxation and wave-packet motion in a ruthenium-based supramolecular photocatalyst, *Chem. Eur. J.*, 2015, **21**, 7668–7674.

19 D. Imanbaew, J. Lang, M. F. Gelin, S. Kaufhold, M. G. Pfeffer, S. Rau and C. Riehn, Pump-Probe Fragmentation Action Spectroscopy: A Powerful Tool to Unravel Light-Induced Processes in Molecular Photocatalysts, *Angew. Chemie - Int. Ed.*, 2017, **56**, 5471–5474.

20 M. J. Frisch, G. W. Trucks, H. B. Schlegel, G. E. Scuseria, M. A. Robb, J. R. Cheeseman, G. Scalmani, V. Barone, B. Mennucci, G. A. Petersson, H. Nakatsuji, M. Caricato, X. Li, H. P. Hratchian, A. F. Izmaylov, J. Bloino, G. Zheng, J. L. Sonnenberg, M. Hada, M. Ehara, K. Toyota, R. Fukuda, J. Hasegawa, M. Ishida, T. Nakajima, Y. Honda, O. Kitao, H. Nakai, T. Vreven, J. J. A. Montgomery, J. E. Peralta, F. Ogliaro, M. Bearpark, J. J. Heyd, E. Brothers, K. N. Kudin, V. N. Staroverov, R. Kobayashi, J. Normand, K. Raghavachari, A. Rendell, J. C. Burant, S. S. Iyengar, J. Tomasi, M. Cossi, N. Rega, J. M. Millam, M. Klene, J. E. Knox, J. B. Cross, V. Bakken, C. Adamo, J. Jaramillo, R. Gomperts, R. E. Stratmann, O. Yazyev, A. J. Austin, R. Cammi, C. Pomelli, J. W. Ochterski, R. L. Martin, K. Morokuma, V. G. Zakrzewski, G. A. Voth, P. Salvador, J. J. Dannenberg, S. Dapprich, A. D. Daniels, O. Farkas, J. B. Foresman, J. V. Ortiz, J. Cioslowski and D. J. Fox, *Gaussian 09, Revision A.02*, Gaussian, Inc., Wallingford CT, 2009.

21 A. D. Becke, Density-functional thermochemistry. III. The role of exact exchange, *J. Chem. Phys.*, 1993, **98**, 5648–5652.

22 C. Lee, W. Yang and R. G. Parr, Development of the Colle-Salvetti correlation-energy formula into a functional of the electron density, *Phys. Rev. B*, 1988, **37**, 785–789.

23 D. Andrae, U. Häußermann, M. Dolg, H. Stoll and H. Preuß, Energy-adjusted ab initio pseudopotentials for the second and third row transition elements, *Theor. Chim. Acta*, 1990, **77**, 123–141.

24 P. C. Hariharan and J. A. Pople, The influence of polarization functions on molecular orbital hydrogenation energies, *Theor. Chim. Acta*, 1973, **28**, 213–222.

25 J. Tomasi, B. Mennucci and R. Cammi, Quantum mechanical continuum solvation models, *Chem. Rev.*, 2005, **105**, 2999–3093.

26 A. D. Laurent and D. Jacquemin, TD-DFT benchmarks: A review, *Int. J. Quantum Chem.*, 2013, **113**, 2019–2039.

27 C. Daniel, Photochemistry and photophysics of transition metal complexes: Quantum chemistry, *Coord. Chem. Rev.*, 2015, **282**–**283**, 19–32.

28 M. Jäger, L. Freitag and L. González, Using computational chemistry to design Ru photosensitizers with directional charge transfer, *Coord. Chem. Rev.*, 2015, **304**–**305**, 146–165.

29 C. Latouche, D. Skouteris, F. Palazzetti and V. Barone, TD-DFT Benchmark on Inorganic Pt(II) and Ir(III) Complexes, *J. Chem. Theory Comput.*, 2015, **11**, 3281–3289.

30 S. Rau, Private communication.

31 H. Torieda, K. Nozaki, A. Yoshimura and T. Ohno, Low quantum yields of relaxed electron transfer products of moderately coupled ruthenium(II)-cobalt(III) compounds on the subpicosecond laser excitation, *J. Phys. Chem. A*, 2004, **108**, 4819–4829.

32 T. Kowacs, L. O'Reilly, Q. Pan, A. Huijser, P. Lang, S. Rau, W. R. Browne, M. T. Pryce and J. G. Vos, Subtle Changes to Peripheral Ligands Enable High Turnover Numbers for Photocatalytic Hydrogen Generation with Supramolecular Photocatalysts, *Inorg. Chem.*, 2016, **55**, 2685–2690.

33 Q. Pan, F. Mecozzi, J. P. Korterik, D. Sharma, J. L. Herek, J. G. Vos, W. R. Browne and A. Huijser, Directionality of ultrafast electron transfer in a hydrogen evolving Ru-Pd-based photocatalyst, *J. Phys. Chem. C*, 2014, **118**, 20799–20806.

34 M. Karnahl, C. Kuhnt, F. Ma, A. Yartsev, M. Schmitt, B. Dietzek, S. Rau and J. Popp, Tuning of photocatalytic hydrogen production and photoinduced intramolecular electron transfer rates by regioselective bridging ligand substitution, *ChemPhysChem*, 2011, **12**, 2101–2109.

35 J. Schindler, Y. Zhang, P. Traber, J.-F. Lefebvre, S. Kupfer, M. Demeunynck, S. Gräfe, M. Chavarot-Kerlidou and B. Dietzek, A ππ* State Enables Photoaccumulation of Charges on a π-Extended Dipyridophenazine Ligand in a Ru(II) Polypyridine Complex, *J. Phys. Chem. C*, 2018, **122**, 83–95.

36 G. E. Shillito, T. B. J. Hall, D. Preston, P. Traber, L. Wu, K. E. A. Reynolds, R. Horvath, X. Z. Sun, N. T. Lucas, J. D. Crowley, M. W. George, S. Kupfer and K. C. Gordon, Dramatic Alteration of 3ILCT Lifetimes Using Ancillary Ligands in [Re(L)(CO)3(phen-TPA)]n+ Complexes: An Integrated Spectroscopic and Theoretical Study, *J. Am. Chem. Soc.*, 2018, **140**, 4534–4542.

37 K. R. A. Schneider, P. Traber, C. Reichardt, H. Weiss, S. Kupfer, H. Görls, S. Gräfe, W. Weigand and B. Dietzek, Unusually Short-Lived Solvent-Dependent Excited State in a Half-Sandwich Ru(II) Complex Induced by Low-Lying 3MC States, *J. Phys. Chem. A*, 2018, **122**, 1550–1559.